AGU PUBLICATIONS

JGR

Journal of Geophysical Research: Space Physics

RESEARCH ARTICLE
10.1002/2015JA021515

Key Points:
- Magnetosphere configuration dramatically changes for sub-Alfvénic/subfast solar wind
- The bow shock disappears, Alfvén wings are formed, and the lobes completely disappear
- The magnetopause expands, the magnetotail shrinks, and the auroral activity greatly diminished

Supporting Information:
- Movie S1
- Movie S1 caption

Correspondence to:
E. Chané,
Emmanuel.Chane@wis.kuleuven.be

Citation:
Chané, E., J. Raeder, J. Saur, F. M. Neubauer, K. M. Maynard, and S. Poedts (2015), Simulations of the Earth's magnetosphere embedded in sub-Alfvénic solar wind on 24 and 25 May 2002, *J. Geophys. Res. Space Physics*, *120*, doi:10.1002/2015JA021515.

Received 2 JUN 2015
Accepted 20 SEP 2015
Accepted article online 8 SEP 2015

Simulations of the Earth's magnetosphere embedded in sub-Alfvénic solar wind on 24 and 25 May 2002

E. Chané[1], J. Raeder[2], J. Saur[3], F. M. Neubauer[3], K. M. Maynard[2], and S. Poedts[1]

[1]Centre for mathematical Plasma Astrophysics, KU Leuven, Leuven, Belgium, [2]Space Science Center, University of New Hampshire, Durham, New Hampshire, USA, [3]Institut für Geophysik und Meteorologie, Universität zu Köln, Cologne, Germany

Abstract During 24 and 25 May 2002, the solar wind conditions at Earth's orbit were very unusual: the density was extremely low (below 0.1/cc) and, as a result, the flow was subfast and sub-Alfvénic (the Alfvén Mach number was as low as 0.4 in the rest frame of the Earth). Consequently, the Earth's bow shock disappeared and two Alfvén wings formed on the flanks of the magnetosphere. These two long structures (estimated extension of 600 R_E for this event) affect the incoming plasma as follows: the velocity is reduced and the magnetic field rotates. In the present study, global magnetohydrodynamical simulations of the magnetosphere are performed for such upstream solar wind conditions. The simulations show how the magnetosphere configuration dramatically changes when the sub-Alfvénic solar wind reaches the magnetosphere: the dayside magnetopause expands up to 20 R_E, and on the nightside the position of the last closed magnetic field line diminishes to 20 R_E. As a result the closed magnetic field line region becomes very symmetric. The open field line configuration also changes such that field lines emanating from the Northern Hemisphere all point in the direction of the dawn Alfvén wing (around 8:00 LT), while the field lines from the Southern Hemisphere all point in direction of the other wing (around 22:00 LT). During the formation of the Alfvén wings, the tail lobes completely disappeared and the auroral activity greatly diminished, i.e., the magnetosphere becomes geomagnetically quiet.

1. Introduction

At the orbit of the Earth, the solar wind is almost always strongly super-Alfvénic and strongly superfast. On average, the Alfvén Mach number (M_A) is equal to 11 [see *Schunk and Nagy*, 2000]. However, on rare occasions the solar wind density is so low that the solar wind becomes sub-Alfvénic. For instance, long periods of sub-Alfvénic solar wind, just upstream of the Earth's magnetosphere were observed on 4 and 31 July 1979, 11 May 1999, 20 March 2002, and 24 and 25 May 2002 [see *Usmanov et al.*, 2005; *Chané et al.*, 2012]. During these sub-Alfvénic solar wind intervals, the Earth's bow shock disappears, and two Alfvén wings are generated on both sides of the Earth. Inside these Alfvén wings, the velocity decreases and the magnetic field rotates. The wings are created by Alfvén waves generated by the interaction between the solar wind and the magnetosphere [see for example, *Neubauer*, 1980, 1998; *Saur et al.*, 1999]. Even though Alfvén wings are not usually present for planets in our solar system (because M_A is almost always larger than one), they are expected to occur at extrasolar planets [see *Shkolnik et al.*, 2003; *Saur et al.*, 2013] and they are observed at planetary satellites, which are embedded in the plasma of their parent planet's magnetosphere [see, for example, *Neubauer*, 1998; *Kivelson et al.*, 2004]. It should also be noted that periods of sub-Alfvénic solar wind are expected to be more frequent at Mercury, where M_A is typically lower than at Earth [*Lavraud and Borovsky*, 2008; *Sarantos and Slavin*, 2009]. The occurrence of sub-Alfvénic events in the solar wind at Earth has been studied by *Usmanov et al.* [2005]. After analyzing 40 years of data, they found only 11 events where the solar wind was sub-Alfvénic.

The observational aspects of the Alfvén wing event at Earth in May 2002 were studied in detail by *Chané et al.* [2012]. As can be seen in Figure 1 (first panel), during this event, the solar wind Alfvén Mach number was extremely low: below 1 for several periods lasting up to 4 h, and even reached a minimum value of 0.4. The low Alfvén Mach number was caused by a very low solar wind density (see second panel). The solar wind density (measured independently by four different spacecraft) was below 0.5 cm^{-3} for at least 40 h and was sometimes as low as 0.04 cm^{-3}. Figure 1 also shows that the solar wind plasma speed was not unusual during

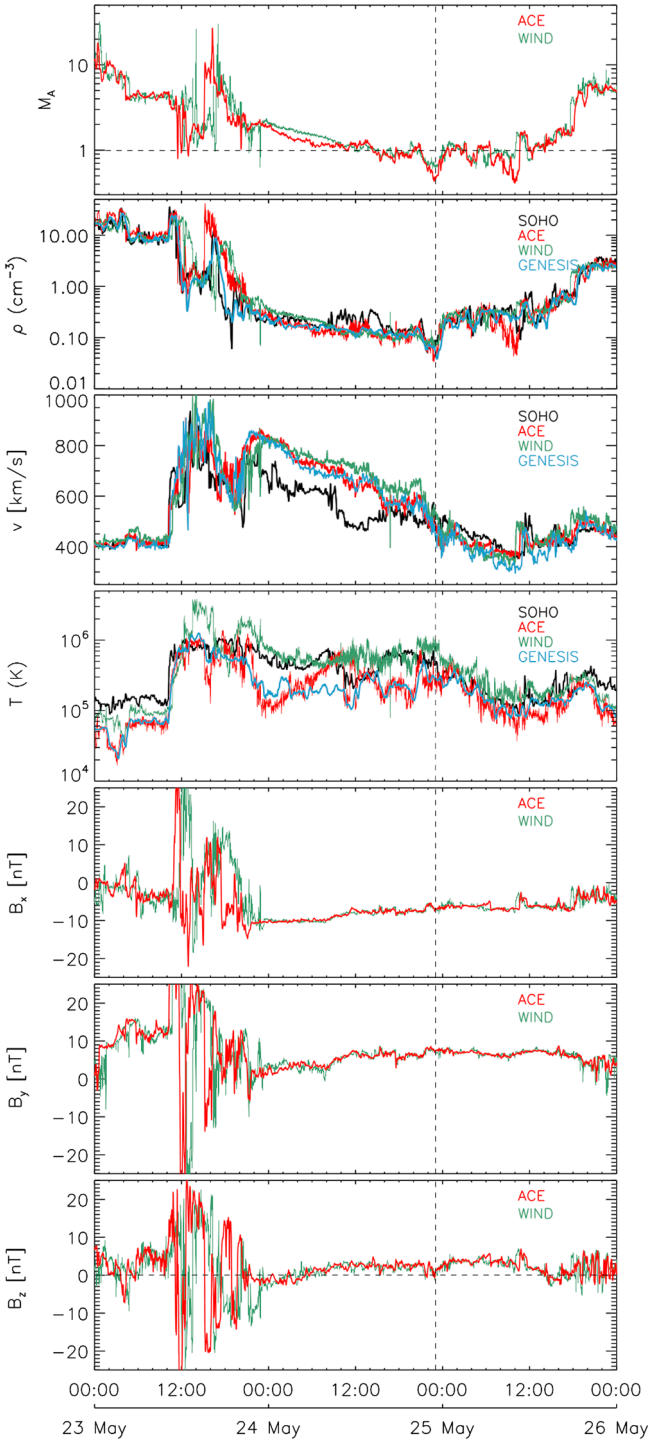

Figure 1. In situ measurements in the solar wind on 24 and 25 May 2002. (first panel) Alfvén Mach number, (second panel) number density, (third panel) plasma speed, (fourth panel) proton temperature, (fifth panel) *X*, (sixth panel) *Y*, and (seventh panel) *Z* component of the magnetic field. The measurements from SOHO, ACE, WIND, and Genesis are displayed in black, red, green, and blue, respectively. A vertical dash line is drawn on 24 May 2002 at 23:00 UTC, this represents the lowest measured Alfvén Mach number during this time interval, and the solar wind parameters measured at that moment are used for the simulations.

this low-density time period, with measured plasma speeds between 300 and 850 km/s. The interplanetary magnetic field was about 10 nT and did not display much fluctuation (see fourth to sixth panels).

The length of the wings was estimated to reach 600 R_E by *Chané et al.* [2012], and the deceleration of the solar wind plasma entering the wings was estimated to be about 30% in one wing and about 60% in the other. The Geotail spacecraft crossed one of the wings several times during this event. Discontinuities in Geotail's measurements were analyzed using the minimum variance analysis. The normals of these discontinuities were found to be perpendicular to the expected wing axis, thus confirming the presence of the wings.

Prior to *Chané et al.* [2012], the magnetosphere-solar wind interaction for extremely tenuous incoming plasma conditions via multispacecraft observations was studied by *Gosling et al.* [1982a]. These authors investigated the magnetosphere configuration on 22 November 1979 when the solar wind density (observed by ISEE 3) was as low as 0.07 cm^{-3}, and the Alfvén Mach number as low as 0.6. During this time interval ISEE 2 was located in the magnetosheath on the dawnside. Surprisingly, according to *Gosling et al.* [1982a, 1982b] ISEE 2 data seem to be consistent with a shock being present between the 2 spacecraft: ISEE 2 measured a stronger magnetic field strength, a higher temperature, and a lower plasma speed than ISEE 3. *Gosling et al.* [1982a] therefore claim that the bow shock did not have sufficient time to dissipate or to move very far upstream. The November 1979 event might thus have been very different from the May 2002 event studied by *Chané et al.* [2012] where the bow shock was gone and where Alfvén wings were demonstrated to be present.

The source of the extremely low density periods in the solar wind remains unclear. *Usmanov et al.* [2005] have shown that the low density on May 1999 could have been caused by a coronal outflow suppression that might be due to a sudden change in the magnetic field of the Sun during the polar field reversal. We note that this is not a possible explanation for the 2002 events since (1) they occurred 2 years after the solar magnetic field reversal and since (2) the low-density region seems to rotate with the Sun and was observed at Earth in March, in May, and in July 2002.

In the present paper, we use global magnetohydrodynamical (MHD) simulations to study the global structure and dynamical evolution of the Earth's magnetosphere for the 24–25 May 2002. It should be noted that during this time period, the upstream conditions (Alfvén Mach number, sonic Mach number, plasma β, etc.) were similar to conditions typically found upstream of Io, Europa, Ganymede, Callisto, and Titan [see *Kivelson et al.*, 2004, Table 21.2]. In the following section, we present the model used for the simulations. In section 3, the results of a simulation with a steady sub-Alfvénic solar wind are discussed. We compare the results of this simulation with the predictions made in *Chané et al.* [2012]. The transition from a super-Alfvénic to a sub-Alfvénic solar wind is studied with another simulation, which is presented in section 4. We show how the magnetotail, magnetopause, and open field lines are affected by this transition The importance of the orientation of the interplanetary magnetic field during sub-Alfvénic upstream conditions is studied in section 5. Finally, our conclusions are presented in section 6.

2. Global MHD Model

OpenGGCM is a global three-dimensional MHD model, which has been used extensively to simulate the interaction between the solar wind and the magnetosphere [see *Raeder et al.*, 1995; *Raeder*, 2003; *Raeder et al.*, 2006, 2008]. It solves the ideal MHD equations in semiconservative form on a nonequidistant mesh. Below a given altitude (2 R_E in the simulations presented here) the model does not solve the MHD equations. Instead, in this so-called *gap region*, a dipole magnetic field is assumed, and the field-aligned electrical current is mapped from the inner boundary down to a sphere of radius 1 R_E. On this sphere, the ionospheric potential equation:

$$\nabla \cdot \underline{\underline{\boldsymbol{\Sigma}}} \cdot \nabla \Phi = -j_{\parallel} \sin I \tag{1}$$

is solved; where $\underline{\underline{\boldsymbol{\Sigma}}}$ represents the ionospheric conductance tensor, Φ the ionospheric potential, $j_{\parallel}$ the mapped field-aligned electrical current, and I the inclination of the dipole field. After solving the potential equation, Φ is mapped up to the inner boundary, where it is used to specify the plasma velocity ($\mathbf{v} = -\nabla\Phi \times \mathbf{B}/B^2$). This method, often referred as the *infinitely thin ionosphere* is broadly used for global simulations of the Earth's magnetosphere [e.g., *Ridley et al.*, 2004; *Zhang et al.*, 2011; *Janhunen et al.*, 2012].

OpenGGCM has been successfully applied to study many aspects of the magnetosphere, for instance, storms [e.g., *Raeder et al.*, 2001a, 2001b], substorms [e.g., *Raeder et al.*, 2010; *Ge et al.*, 2011], the cold dense plasma layer [e.g., *Li et al.*, 2009], and flux transfer events [e.g., *Raeder*, 2006].

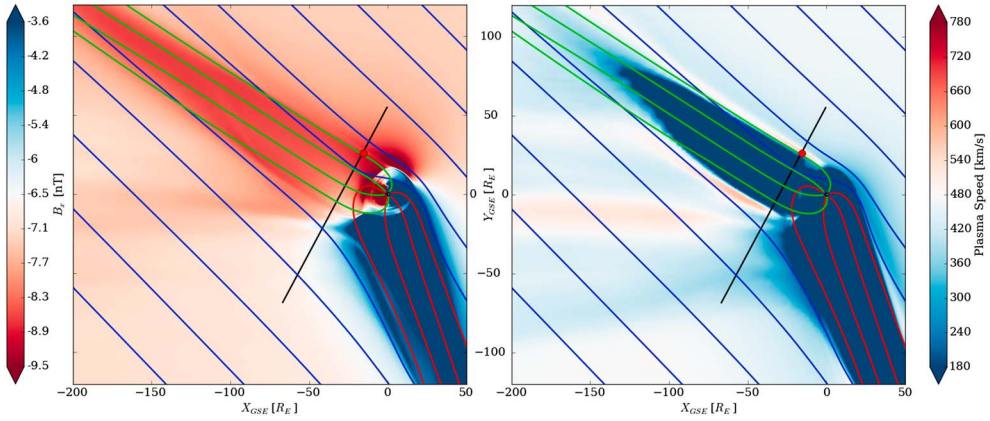

Figure 2. Top view (left) of the field lines and color coded B_x and (right) of the plasma speed in the equatorial plane for simulation 1 7 h after the simulation was started. The solar wind is coming from the right. The magnetic field lines are shown in red when connected to the northern ionosphere, in green when connected to the southern ionosphere, and in blue when not connected to the Earth's ionosphere. The black line shows a plane across the dusk Alfvén wing displayed in Figure 3. The red dot represents the position of Geotail on 24 May 2002 at 23:00 UTC. Note that values of B_x below −9.5 nT are all displayed with the same color (dark red), values of B_x above −3.6 nT are all displayed with one unique color (dark blue), and values of V below 180 km/s are all displayed with the same color (dark blue).

In the present study, we use a mesh with slightly more than 327 million cells (496 × 812 × 812). The dayside outer boundary is located 400 R_E upstream of the Earth, while the five other outer boundaries are located 1000 R_E from Earth (where outflow boundary conditions are applied). The smallest cells (i.e., close to the inner boundary) are approximately 0.4 R_E wide. For simplicity the ionospheric Pedersen and Hall conductances are assumed to be constant and equal to 5 S.

3. Global Simulation With a Steady Sub-Alfvénic Inflow

For simulation 1, we consider a constant sub-Alfvénic ($M_A = 0.4$) incoming solar wind, with a density $n = 0.04$ cm^{-3}, a velocity $v_x = -480$ km/s, a thermal plasma pressure $p = 0.29$ pPa and a constant interplanetary magnetic field given by $\mathbf{B} = (-7.2, 7.3, 1.0)$ nT (GSE coordinate system), which correspond to a plasma β of 0.007, to a sonic Mach number M of 5.6, and to a plasma temperature T of ∼260,000 K (we assume $p = 2nkT$, where k is the Boltzmann constant). These values were measured by ACE on 24 May 2002 at 23:00 UTC, i.e., during an extremely low density time period, as can be seen in Figure 1 (highlighted by the vertical dashed line).

Figure 2 shows the magnetic field (field lines and X component of the field) and the plasma speed for this run, 7 h after the simulation was started. The two Alfvén wings can clearly be seen on the flank of the Earth in this figure, with an enhancement of B_x in the dawn wing and a drop in the dusk wing, whereas the plasma speed drops in both wings. The orientation of the wings depends on the incoming solar wind plasma velocity and Alfvén velocity and is given by $\mathbf{C_A^{\pm}} = \mathbf{v} \pm \mathbf{v_A}$ [see *Neubauer*, 1980]. For the solar wind values considered in this simulation, the wings should point to 21:52 LT and 07:23 LT, which is exactly reproduced in the simulation. The wings propagate with the velocity $\mathbf{C_A^{\pm}}$ away from the Earth. Thus, after 30 min they should extend up to $Y = \pm 222$ R_E. This is exactly what happens in the simulation (not shown here). The three-dimensional field line structure is not readily visible in Figure 2, and these field lines are not constrained to the equatorial plane. For example, the field lines emanating from the northern ionosphere (displayed in red) extend northward at first and reach distances above the equatorial plane as large as 12 R_E. These field lines form the dawn Alfvén wing, pointing slightly southward at large distances. When these field lines reach the border of Figure 2 (for $Y = -120$ R_E) they are between 5 R_E and 21 R_E south of the equatorial plane. The opposite happens with the field lines coming from the southern ionosphere (displayed in green): they extend southward at first (as low as 15 R_E below the equatorial plane) and then bend northward to form the wing. When these field lines reach the border of the figure ($X = -200$ R_E) they are between 8 R_E and 18 R_E north of the equatorial plane.

The analytical models of *Neubauer* [1980] and *Saur et al.* [1999] predict that, for this simulation, B_x should be −8.47 nT in the dusk wing and −4.65 nT in the dawn wing, because the field lines are partially rotated toward

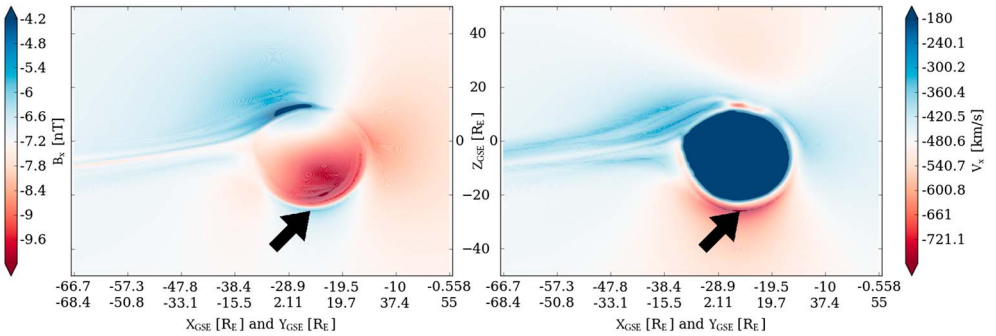

Figure 3. *X* component (top) of the magnetic field and (bottom) of the plasma velocity in a plane perpendicular to the dusk Alfvén wing (shown in black in Figure 2). Saturated color bars are used: values below −10.2 nT and below −780 km/s are shown with a unique color (dark red), values above −4.2 nT and above −180 km/s in dark blue. The minimum and maximum values for v_x in this plane are −793 km/s and −30 km/s, respectively. B_x is as low as −10.3 nT and as high as −2.9 nT. The black arrows point to a region just outside of the Alfvén wing, where the plasma speed and B_x are larger than in the solar wind.

the axes of the wings. The simulations are in good agreement with this prediction: in the center of the wings, we find $B_x \in [-9.0, -8.8]$ nT and $B_x \in [-4.0, -2.8]$ nT for the dusk and for the dawn wing, respectively.

In *Chané et al.* [2012], we found several time intervals when Geotail measured higher plasma speeds and a larger *X* component of the magnetic field than in the solar wind (see Figure 4 (bottom)), which is consistent with Geotail being outside the inner region of the Alfvén wing (the inner part of the Alfvén wing is the cylindrical region where the standing Alfvén waves generated in the ionosphere travel). In the inner wing the plasma would be expected to be decelerated and not accelerated. We therefore suggested in that paper that Geotail was possibly located just outside of the inner Alfvén wing, on the flank, because the plasma would be accelerated around the wings and because B_x can be increased there [see *Neubauer*, 1980]. Such higher speeds and a larger *X* component of the magnetic field are indeed observed in simulation 1, where the plasma speed just outside of the dusk Alfvén wing is up to 300 km/s higher and B_x is up to 2 nT larger than in the solar wind (as highlighted by the black arrows in Figure 3).

A direct comparison between the simulation results and Geotail's data is of course not possible here, since we used constant solar wind conditions in the simulation. As a matter of fact, the Alfvén wing crossings observed by Geotail are not caused by the spacecraft moving through a static wing, but caused by the wing moving past an almost stationary spacecraft. Furthermore, the wings moved because the solar wind conditions were changing. It is therefore difficult to exactly pinpoint where the Alfvén wing crossings may have happened in Figure 3. We provide a vertical and a horizontal cut through the simulated wing in Figure 4 (top) which mimic more or less how an Alfvén wing crossing would look like if the wing was moving horizontally or vertically. We show v_x in red and B_x in blue. The dark background shows the position of the inner Alfvén wing and the white background of the outer Alfvén wing. These cuts are compared with Geotail's data during Alfvén wing crossing (lower panel). Our results are in qualitative agreement with Geotail observations: inside the wing, B_x is more negative and the plasma speed is lower than in the solar wind (the solar wind plasma speed is 480 km/s). In addition, there are locations where the plasma is faster than in the solar wind (top panel at the edge between the inner and the outer wing). For the inner Alfvén wing: B_x is between −9 nT and −7 nT for Geotail's data, and these values are also observed in our simulations (where B_x is as low as −10.3 nT); while the measured v_x is about −300 km/s and such values are also present in the simulations (where the plasma speed can be as low as 30 km/s). However, we do not reproduce the outer Alfvén wing as well: in the simulations, the highest values for B_x are −2.9 nT, while positive values were clearly measured by Geotail. It is not surprising that our simulation is not in perfect agreement with Geotail's observations, since we performed a steady state simulation with constant solar wind conditions: anything that is caused by variations in the solar wind cannot be reproduced in our simplified simulation.

In the literature, the Alfvén wings are often depicted in a plane containing the magnetic field vector, the velocity vector of the incoming flow and the central body: this is the plane of the two wings. In this plane, one can clearly see the deceleration of the plasma flow inside the wings, but cannot see its acceleration around the wings (which happens outside of the plane). Nevertheless, the acceleration of the plasma around the wings is

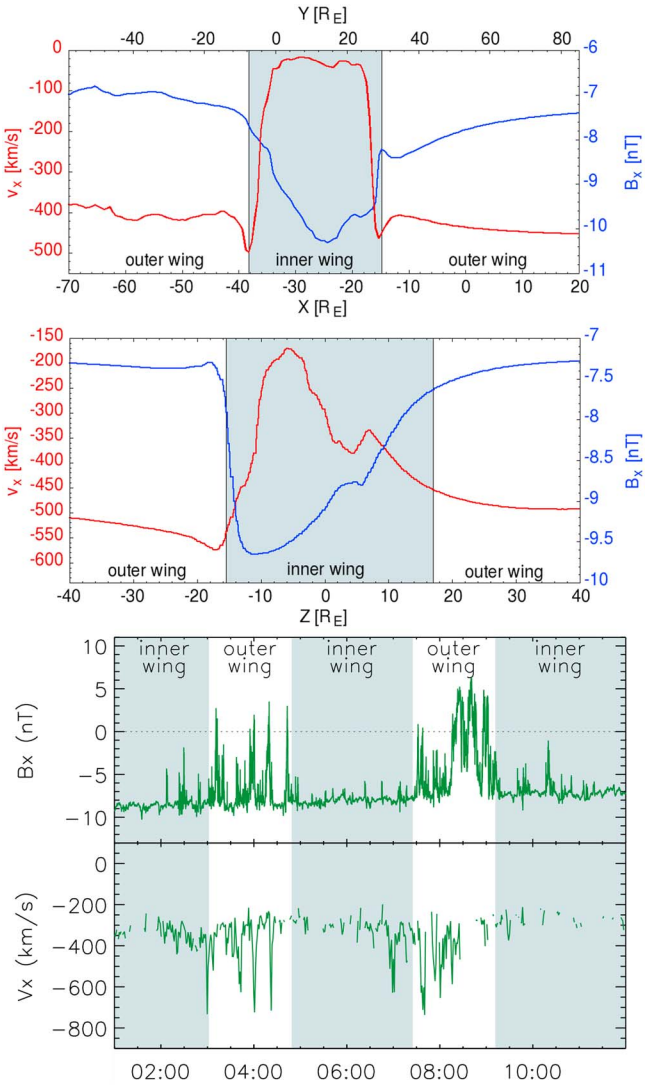

Figure 4. Comparison between (top and middle) simulation results and (bottom) Geotail's in situ measurements on 25 May 2002 . Figure 4 (top) is a horizontal cut through the wing ($Z = -10\ R_E$), while Figure 4 (middle) is a vertical cut through the wing ($X = -15.27\ R_E$, $Y = 26.27\ R_E$). The X component of the magnetic field and of the velocity are displayed in blue and in red, respectively. The background color represents the position of the spacecraft: dark for the inner Alfvén wing and white for the outer Alfvén wing (i.e., the region just outside of the inner wing).

real and has been described by theory, observations, and numerical simulations [e.g., *Saur et al.*, 1999; *Frank and Paterson*, 2000; *Schilling et al.*, 2008; *Jia et al.*, 2009]. For instance, in the simulations of the Alfvén wings at Earth performed by *Ridley* [2007], plasma speeds faster than in the solar wind cannot be seen because only the plane of the Alfvén wings is shown: nevertheless, these high speeds are most probably present in the simulations and are likely similar to our simulation as shown in Figure 3.

While simulation 1 is useful at first to obtain a global insight of the magnetosphere during the 24 and 25 May 2002, and to compare the results with our predictions [*Chané et al.*, 2012], it excludes the transition from the super-Alfvénic to the sub-Alfvénic regime, when the bow shock disappears, and the Alfvén wings unfold.

4. Transition From a Super-Alfvénic to a Sub-Alfvénic Solar Wind

The second simulation addresses the transition that the magnetosphere undergoes when the solar wind becomes sub-Alfvénic. The transition to sub-Alfvénic interaction was also studied by *Ridley* [2007] but under very different conditions. In that study the sub-Alfvénic solar wind flow was caused by an extremely strong interplanetary magnetic field, which is different from the May 2002 case, where the sub-Alfvénic flow was

Table 1. Position of the Subsolar Bow Shock as a Function of Time for Simulation 2[a]

Position of the Shock (R_E):	20	30	40	60	90
Time	3 h 19 min	3 h 26 min	3 h 30 min	3 h 35 min	3 h 40 min

[a]Note that the solar wind density just upstream of the magnetosphere linearly decreases from $t = 2$ h 50 min to $t = 3$ h 50 min.

caused by an unusually low solar wind density. We start the simulation with a solar wind number density of $n = 5$ cm^{-3}, a velocity of $v_x = -480$ km/s, a temperature of $T = 260,000$ K, and an interplanetary magnetic field of $\mathbf{B} = (-7.2, 7.3, 1.0)$ nT. These values correspond to a solar wind Alfvén Mach number of 4.8. These parameters are kept constant for the first 2 h of the run. After that, the solar wind density linearly decreases for 1 h to a value of 0.04 cm^{-3}, which corresponds to a solar wind Alfvén Mach number of 0.4. Subsequently, the solar wind is kept constant for the remainder of the simulation. For simplicity, we chose a linear transition as opposed to something more closely representative of the May 2002 case in Figure 1. The study of the full 3-D development of a larger environment of the Earth on a large-scale involving solar wind dynamics is outside the scope of this work.

An animation showing B_x and selected magnetic field lines in the equatorial plane for simulation 2 is included in the supporting information of this paper. Solar wind field lines are displayed in blue, open field lines that connect to the Northern (Southern) Hemisphere in red (green), and closed field lines in gray. One can see how the bow shock starts to move sunward around 3 h 10 min, when the low-density solar wind reaches the magnetosphere. Table 1 shows how the position of the bow shock varies with time. The shock moves rapidly away from the Earth and in tens of minutes already reaches speeds of more than 600 km/s. While moving away, the shock becomes weaker because (1) of the nature of the fast waves that propagate in every direction, and since (2) the numerical mesh is coarser far away from the Earth, which causes numerical dissipation and broadening of the shock (the cells' sizes rapidly increase around 60 R_E: $\Delta x = 0.8$ R_E at 75 R_E, $\Delta x = 1.6$ R_E at 85 R_E, $\Delta x = 5$ R_E at 100 R_E, and $\Delta x = 9$ R_E at 200 R_E). Since the shock fades away when it moves outward, it becomes very hard to pinpoint its exact location beyond 100 R_E. Nevertheless, we see that it propagates up to the outer boundary at 400 R_E and that it bounces back in the direction of the Earth at 4 h 5 min. But at that point, the shock is so weak that it is almost impossible to detect and, as a result, does not affect our solution. The issue of waves reflecting at the boundaries for Alfvén wing simulations was discussed in detail by *Ridley* [2007]. He proposed the following so that the waves' reflection at the boundaries would not affect the simulation: (1) move the boundary far away, (2) run the simulation only for small periods of time, or (3) modify the boundary conditions to absorb backward propagating waves. His first and second propositions have the same effect: the waves generated in the ionosphere have no time to reach the boundary and to come back in the region of interest. The mesh we use in our simulations is chosen to avoid reflection of waves at the boundaries that could affect the results: (1) the outer boundaries are far from the Earth and it takes therefore a very long time for the waves to reach them and (2) the mesh is very coarse close to the outer boundary and, as a result, the waves are damped.

The movie shows how, for the dawn Alfvén wing, the solar wind field lines reconnect with either closed field lines or field lines from the magnetotail to form the dawn Alfvén wing. This can clearly be seen at 3 h 53 min 20 s, 3 h 54 min, 4 h 2 min 20 s, 4 h 23 min, and 4 h 47 min 40 s. On the other hand, field lines from the dusk Alfvén wing are mostly, field lines from the magnetotail that slowly move to the dusk Alfvén wing; this is because, in this simulation, the magnetotail and the dusk Alfvén wing are relatively close to each other. This animation also shows how stable the Alfvén wing magnetic field lines are in the simulation once the wing has fully developed (after 4 h 40 min): this indicates that in our simulations the plasma speed inside the wing becomes very low. During the last hour of this animation, one can see that the field lines plotted in the dawn Alfvén wings are only slightly displaced tailward (between 3.8 R_E and 16 R_E).

Figure 5 shows the magnetic field configuration of the magnetosphere for simulation 2 after 3.0 h (left column), just before the sub-Alfvénic solar wind reaches the magnetosphere, and after 5.5 h, when the flow has become sub-Alfvénic at Earth (right column). Figure 5 (top row) shows the closed field lines, and Figure 5 (bottom row) shows the open field lines. The magnetic field topology changes profoundly when the solar wind Alvén Mach number decreases. First, the magnetotail contracts. The last closed field lines on the nightside move from more than 101 R_E to approximately 20 R_E. By contrast, on the dayside the magnetopause is moving sunward, because the solar wind ram pressure decreases. While the last closed magnetic field lines

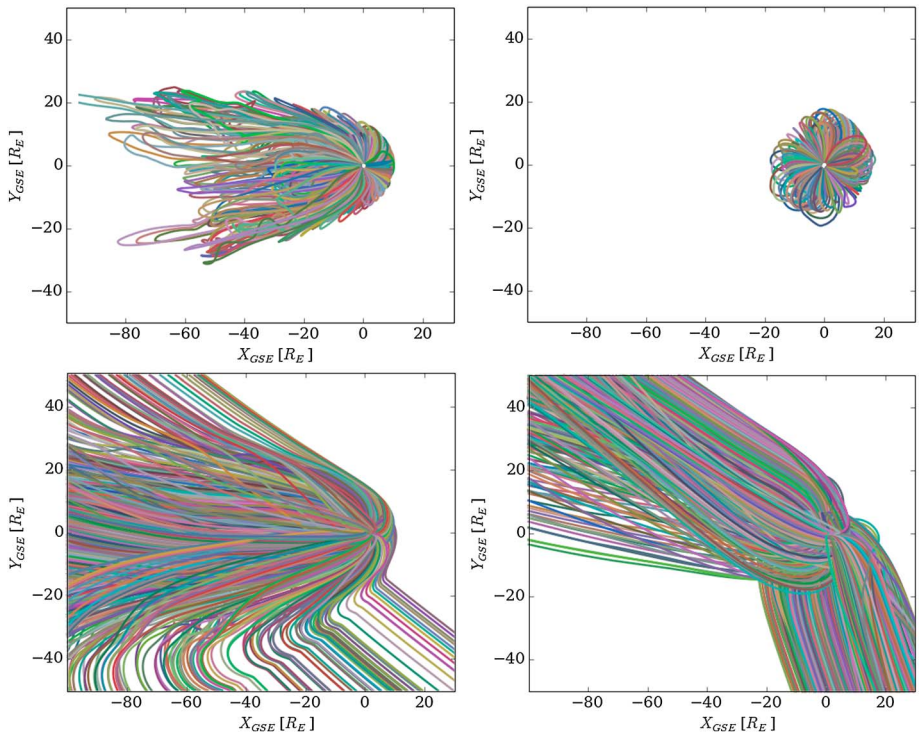

Figure 5. Top view of the magnetic field lines in simulation 2. (top row) Closed magnetic field lines. (bottom row) Open magnetic field lines (only one side is connected to the ionosphere). (left column) Three hours after the simulation started (the sub-Alfvénic flow did not reach the Earth's magnetosphere yet). (right column) 5.5 h after the simulation started (the Earth's magnetosphere is embedded in a sub-Alfvénic solar wind). The solar wind is coming from the right. The colors of the magnetic field lines have no specific meaning.

where located around 13 R_E when the solar wind was super-Alfvénic, they extend to approximately 20 R_E when the solar wind becomes sub-Alfvénic. Thus, the closed magnetic field line region is more symmetric when the solar wind is sub-Alfvénic. This is consistent with the conclusions from *Le et al.* [2000], who claim that the magnetosphere is much more dipolar than usual when embedded in a low-density solar wind. Their conclusions are based on measurements from the Polar spacecraft during the 11 May 1999 event (usually referred to as "the day the solar wind almost disappeared"). As the solar wind ram pressure strongly decreases, the solar wind magnetic pressure plays a more important role. While the solar wind ram pressure tends to decrease the size of the magnetosphere on the dayside and to increase it on the nightside, the solar wind magnetic pressure decreases its size on both the dayside and the nightside (note that the magnetic forces only act in the direction perpendicular to the magnetic field, this may flatten the magnetosphere, see *Sibeck et al.*, 1986). The ratio between ram ($\rho_{sw} v_{sw}^2$) and magnetic ($B_{sw}^2/(2\mu_0)$) pressure is given by $2{M_A}^2$. During the first part of the simulation this ratio is 46, and the solar wind magnetic pressure is negligible in comparison with the solar wind ram pressure. On the other hand, at the end of the simulation, when the solar wind density in the simulation is 0.04 cm^{-3}, this ratio is 0.36; meaning that the magnetic pressure is 2.8 times stronger than the ram pressure and plays the dominant role in shaping the magnetosphere.

Second, the geometry of the open magnetic field lines also changes dramatically when the solar wind becomes sub-Alfvénic (see Figure 5 (bottom row)). At the beginning of the simulation, the open field lines either connect to the lobes or are bent into the equatorial plane and connect to the interplanetary magnetic field. But when the solar wind is sub-Alfvénic, the open field lines emanating from the Earth's ionosphere connect to the Alfvén wings. The open field lines from the Northern Hemisphere connect to the dawn wing (around 8:00 LT), and open field lines from the Southern Hemisphere connect to the dusk wing (around 22:00 LT). Note that regardless of the orientation of the interplanetary magnetic field and solar wind velocity, the field lines emanating from the Northern Hemisphere always connect to one wing ($\mathbf{v} - \mathbf{v_A}$) and the field lines from the Southern Hemisphere to the other wing ($\mathbf{v} + \mathbf{v_A}$).

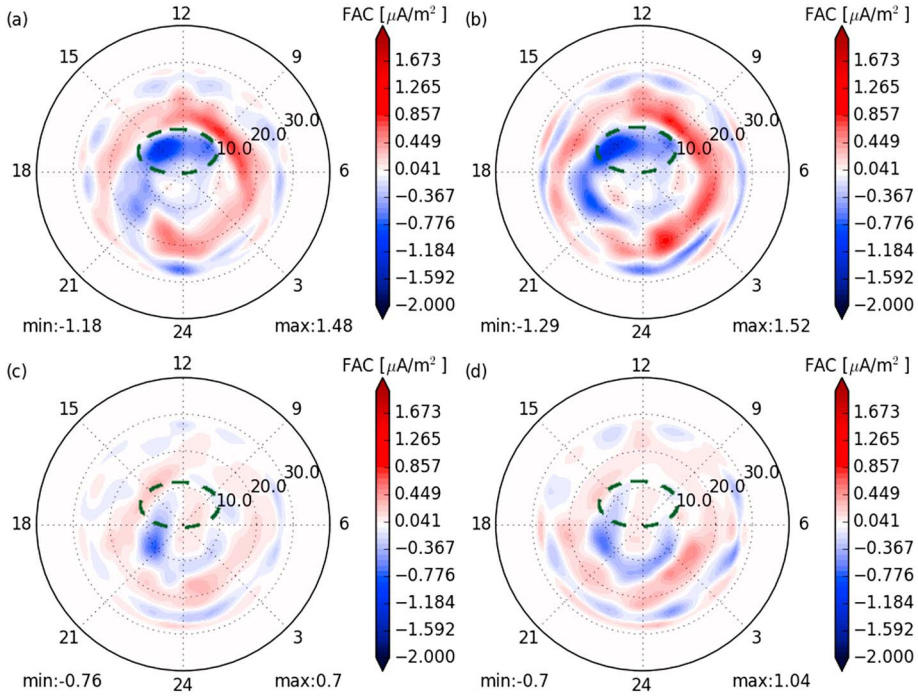

Figure 6. Polar projection of the field-aligned currents in the northern ionosphere for simulation 2 and 3. Upper panels: 2 h after the simulation started (before the sub-Alfvénic flow reaches the magnetosphere). Lower panels: 5 h after the simulation started (sub-Alfvénic solar wind). Left panels: simulation 2 (positive B_z in the solar wind). Right panels: simulation 3 (negative B_z in the solar wind). The dashed green ovals highlight the disappearance of the cusp current when the solar wind becomes sub-Alfvénic in the simulations. Local noon is at the top of each panel.

Figure 5 also shows how the lobes disappear when the solar wind becomes sub-Alfvénic, and how they are replaced by the Alfvén wings. The same effect was shown by *Ridley* [2007], for example, in Figure 7 of that paper. In that simulation, the lobes are also progressively transformed into Alfvén wings when the Alfvén Mach number decreases. However, in the Ridley simulation, the interplanetary magnetic field lies in the noon-midnight equatorial plane. Thus, in that simulation it appears that the lobes merely fan out and the plasma sheet disappears. Since our simulation also includes an east-west interplanetary magnetic field component, the Alfvén wings are also bent into the dawn and dusk directions, respectively.

In Figure 5 (bottom right), some of the field lines emanating from the southern ionosphere are not exactly pointing in the direction of the dusk wing. This is a transient phenomenon. These field lines are still moving from the lobe into the wing; 150 min later all open field lines point exactly in the direction of wings. Figure 5 shows how drastically the magnetic field pattern changed in only 2.5 h, but one should keep in mind that this pattern is still (slowly) changing for 150 min (meaning that it took 5 h to the magnetosphere to fully adjust to the new solar wind conditions).

Figure 6 (left column) shows how the field-aligned currents in the ionosphere change as the solar wind becomes sub-Alfvénic in simulation 2. First, the magnitude of the strongest field-aligned currents decreases by about 45%. We also integrated the upward electrical current at the inner boundary for both hemispheres and found that it decreased from 6.5 MA when the solar wind was super-Alfvénic to 3 MA when it is sub-Alfvénic. Second, the field-aligned current pattern changes. During super-Alfvénic flow, the pattern is the well-known region-1/2 pattern that is expected when the interplanetary magnetic field is duskward as in this simulation. In particular, the strongest field-aligned current is an upward current right under the cusp. Since the interplanetary magnetic field is slightly northward, there is no substorm activity, and the nightside field-aligned current is weak. The field-aligned current pattern changes significantly when the solar wind flow turns sub-Alfvénic. The cusp currents disappear, and instead the strongest field-aligned current is an upward current that should connect to the dawnward Alfvén wing. The weak field-aligned currents in this simulation are consistent with the disappearance of auroral activity during this event as reported by *Chané et al.* [2012].

One should keep in mind that, in our simulation, the transition from super-Alfvénic to sub-Alfvénic solar wind conditions was obtained by decreasing the solar wind density (since this is what happened during the May 2002 event) while the interplanetary magnetic field was kept constant. The ionospheric current would be different if the sub-Alfvénic conditions would have been caused by a strong interplanetary magnetic field. This can be seen in *Ridley* [2007] where the field-aligned currents increase by a factor of 3 when the solar wind becomes sub-Alfvénic. In these simulations the strength of the interplanetary magnetic field was multiplied by 20 to obtain the sub-Alfvénic incoming flow. So the weak ionospheric currents in the May 2002 event are primarily caused by the decrease of the solar wind density. In contrast, *Le et al.* [2000], after analyzing the data from the Polar spacecraft in May 1999, concluded that the field-aligned currents are almost not affected by the solar wind dynamic pressure.

5. Importance of the Orientation of the Interplanetary Magnetic Field

At the end of simulation 2, the field-aligned currents in the ionosphere are weak, indicating that the reconnection rate at the dayside magnetopause is low. However, since the interplanetary magnetic field is directed northward in this simulation, this reconnection rate is expected to be low and we cannot be certain that this is caused by the sub-Alfvénic solar wind. We therefore performed a third simulation, which is the same as simulation 2, except for the sign of B_z in the solar wind: $\mathbf{B} = (-7.2, 7.3, -1.0)$ nT.

While the results of simulations 2 and 3 are significantly different at first (when the solar wind is still super-Alfvénic), they become very similar once the solar wind is sub-Alfvénic. For instance, 3 h after the beginning of the simulations (before the sub-Alfvénic flow reaches the Earth's magnetosphere), the magnetotail is 50% shorter in simulation 3 than in simulation 2 (not shown here). As can be seen in Figure 6, during the first part of the simulations, for both runs, the field-aligned currents in the ionosphere display the well-known region-1/2 pattern (because the interplanetary magnetic field is duskward); however, the field-aligned current patterns are not identical for both runs, and the currents are slightly stronger on the nightside for simulation 3, which is expected for a southward interplanetary magnetic field and is caused by substorm activity. Once the solar wind becomes sub-Alfvénic, the field lines configurations are almost identical for both simulations. The only difference is that whereas the dawn and dusk Alfvén wings point slightly northward and southward respectively in simulation 3, they point slightly southward and northward respectively in simulation 2 (which is expected when one switches B_z in the interplanetary magnetic field). For both simulations, the ionospheric field-aligned currents are similar and are very weak in comparison with values during usual solar wind conditions. The nightside downward currents are about 30% weaker for simulation 2, which indicates that the reconnection rate in the tail is higher (although still very weak) in simulation 3.

For very low Alfvén Mach number and strong reconnection, the theoretical expectation for the difference in the total Alfvén wing current between simulations 2 and 3 is approximately 5%. This difference is calculated with the expressions in Figure 7 in *Saur et al.* [2013] and the currents for an elliptically shaped wing in *Saur* [2004]. The change in total Alfvén wing current is small because the change in orientation of the interplanetary magnetic field is only about 10° between simulation 2 and 3. The weak change in the orientation of the external field only weakly modifies the geometry of the Alfvén wings, which is very similar to the results of our simulations.

6. Discussions and Conclusions

In this article, we presented the results of three global MHD simulations of the Earth's magnetosphere embedded in a sub-Alfvénic solar wind, similar to the 24 and 25 May 2002 event. We find that

1. The simulations are in good qualitative agreement with the observations and theoretical predictions. In particular, the orientation of the wings agrees very well with theory *Neubauer* [1980]. In places where data were available from the Geotail observations [*Chané et al.*, 2012], e.g., the magnetic field within the Alfvén wing, there is also good quantitative agreement.
2. We also find a region of higher plasma speed and larger B_x just outside of the wings, which is in agreement with the interpretation of the observations made by *Chané et al.* [2012].
3. The simulation shows that the magnetic field topology changes profoundly when the solar wind becomes sub-Alfvénic. The tail lobes disappear and turn into Alfvén wings. The wings are not aligned antisunward, as the lobes are, but their orientation is given by the interplanetary magnetic field and by the solar wind velocity and density. For the particular event selected here, the wings point to 21:52 LT and 07:23 LT.

4. Because the ratio between the solar wind ram pressure and magnetic pressure decreases as the square of the Alfvén Mach number, the shape of the magnetosphere is primarily determined by the magnetic pressure of the interplanetary magnetic field rather than the ram pressure. Thus, the magnetosphere expands on the dayside and contracts on the nightside. Although in the case considered here the low Mach number was caused by low density, this effect should occur regardless of what causes the low Mach number, e.g., low solar wind density, strong interplanetary magnetic field, low solar wind speed, or a combination thereof. Because the magnetic Lorentz force acts perpendicular to the magnetic field and is null parallel to the magnetic field, the magnetosphere may also become flattened in the direction perpendicular to the magnetic field. This has been observed in the distant magnetotail *Sibeck et al.* [1986], where less magnetic pressure is required to have such an effect [see also *Lavraud et al.*, 2007, 2013].
5. The magnetosphere becomes geomagnetically quiet during the sub-Alfvénic solar wind interval. Because geomagnetic activity is primarily driven by magnetic reconnection at the dayside magnetopause, this implies that reconnection has ceased, or at least has diminished to the point where it plays no significant role any more. However, this statement should not be generalized, because in the cases considered here, the interplanetary magnetic field had a northward B_z component for simulation 2 or a weak southward B_z for simulation 3. Geomagnetic activity may or may not be stronger if the interplanetary magnetic field had a stronger southward component.

It should be noted that the results obtained in the present article are for an extremely tenuous solar wind (0.04 cm^{-3}), resulting in a very low Alfvén Mach number (0.4). Even though such a low density was measured by ACE on 24 May 2002 at 23:00 UTC, one should keep in mind that this was the lowest Alfvén Mach number measured during this event. Nevertheless, long periods of sub-Alfvénic solar wind with a somewhat larger Alfvén Mach number (as were also measured during this event) should produce qualitatively similar results. For instance, for values of M_A above 0.4, the magnetotail might not shrink as strongly and the wing would not point in the exact same direction, but, there would be no bow shock (as long as the incoming flow is subfast), and Alfvén wings would form, affecting the plasma and field that flow through them and close to them. It is also important to remember that the solar wind conditions are never as steady as the one used in these two simulations. Due to variations in the solar wind density, velocity, and magnetic field, the wings would never be as straight as they appear in Figures 2 and 5.

Finally, it remains an open question how reconnection might affect the structure of Alfvén wings. Determining the reconnection topology in gridded data from three-dimensional simulations is notoriously difficult [*Raeder and Germaschewski*, 2012] and will be deferred to future study. Unfortunately, such low Alfvén Mach number events rarely occur in the solar wind. Thus, global simulations will remain the primary tool to study Alfvén wings at Earth.

Acknowledgments
The simulation data of this paper are available upon request. Work at UNH was supported by grant NNX10AL07G from the National Aeronautics and Space Administration and by grant AGS-1143895 from the National Science Foundation. Work at the University of Cologne was supported by the Schwerpunktprogramm "Planetary Magnetism" of the Deutsche Forschungsgemeinschaft under grant SA 1772/1-2. Work at KUL has been funded by the Interuniversity Attraction Poles Programme initiated by the Belgian Science Policy Office (IAP P7/08 CHARM), by grant GOA/2015-014 from the Geconcerteerde Onderzoeksacties, and by the Research Foundation-Flanders (FWO 12M0115N). Computations were performed on Stampede at the Texas Advanced Computing Center and on Trillian, a Cray XE6m-200 supercomputer at UNH supported by the NSF MRI program under grant PHY-1229408. We thank B. Lavraud for useful discussions and for his comments on the manuscript.

Yuming Wang thanks Andrey Samsonov and one other reviewer for their assistance in evaluating this paper.

References

Chané, E., J. Saur, F. M. Neubauer, J. Raeder, and S. Poedts (2012), Observational evidence of Alfvén wings at the Earth, *J. Geophys. Res.*, *117*, A09217, doi:10.1029/2012JA017628.

Frank, L. A., and W. R. Paterson (2000), Return to Io by the Galileo spacecraft: Plasma observations, *J. Geophys. Res.*, *105*, 25,363–25,378, doi:10.1029/1999JA000460.

Ge, Y. S., J. Raeder, V. Angelopoulos, M. L. Gilson, and A. Runov (2011), Interaction of dipolarization fronts within multiple bursty bulk flows in global MHD simulations of a substorm on 27 February 2009, *J. Geophys. Res.*, *116*, A00I23, doi:10.1029/2010JA015758.

Gosling, J. T., J. R. Asbridge, S. J. Bame, W. C. Feldman, R. D. Zwickl, G. Paschmann, N. Sckopke, and C. T. Russell (1982a), A sub-Alfvenic solar wind—Interplanetary and magnetosheath observations, *J. Geophys. Res.*, *87*, 239–245, doi:10.1029/JA087iA01p00239.

Gosling, J. T., J. R. Asbridge, S. J. Bame, W. C. Feldman, G. Paschmann, N. Sckopke, and C. T. Russell (1982b), Evidence for quasi-stationary reconnection at the dayside magnetopause, *J. Geophys. Res.*, *87*, 2147–2158, doi:10.1029/JA087iA04p02147.

Janhunen, P., M. Palmroth, T. Laitinen, I. Honkonen, L. Juusola, G. Facskó, and T. I. Pulkkinen (2012), The GUMICS-4 global MHD magnetosphere-ionosphere coupling simulation, *J. Atmos. Sol. Terr. Phys.*, *80*, 48–59, doi:10.1016/j.jastp.2012.03.006.

Jia, X., R. J. Walker, M. G. Kivelson, K. K. Khurana, and J. A. Linker (2009), Properties of Ganymede's magnetosphere inferred from improved three-dimensional MHD simulations, *J. Geophys. Res.*, *114*, A09209, doi:10.1029/2009JA014375.

Kivelson, M. G., F. Bagenal, W. S. Kurth, F. M. Neubauer, C. Paranicas, and J. Saur (2004), Magnetospheric interactions with satellites, in *Jupiter. The Planet, Satellites and Magnetosphere*, edited by F. Bagenal, T. E. Dowling, and W. B. McKinnon, pp. 513–536, Cambridge Univ. Press, Cambridge, U. K.

Lavraud, B., and J. E. Borovsky (2008), Altered solar wind-magnetosphere interaction at low Mach numbers: Coronal mass ejections, *J. Geophys. Res.*, *113*, A00B08, doi:10.1029/2008JA013192.

Lavraud, B., J. E. Borovsky, A. J. Ridley, E. W. Pogue, M. F. Thomsen, H. Rème, A. N. Fazakerley, and E. A. Lucek (2007), Strong bulk plasma acceleration in Earth's magnetosheath: A magnetic slingshot effect?, *Geophys. Res. Lett.*, *34*, L14102, doi:10.1029/2007GL030024.

Lavraud, B., et al. (2013), Asymmetry of magnetosheath flows and magnetopause shape during low Alfvén Mach number solar wind, *J. Geophys. Res. Space Physics*, *118*, 1089–1100, doi:10.1002/jgra50145.

Le, G., C. T. Russell, and S. M. Petrinec (2000), The magnetosphere on May 11, 1999, the day the solar wind almost disappeared: I. Current systems, *Geophys. Res. Lett.*, *27*, 1827–1830, doi:10.1029/1999GL010774.

Li, W., J. Raeder, M. Øieroset, and T. D. Phan (2009), Cold dense magnetopause boundary layer under northward IMF: Results from THEMIS and MHD simulations, *J. Geophys. Res.*, *114*, A00C15, doi:10.1029/2008JA013497.

Neubauer, F. M. (1980), Nonlinear standing Alfven wave current system at Io: Theory, *J. Geophys. Res.*, *85*, 1171–1178, doi:10.1029/JA085iA03p01171.

Neubauer, F. M. (1998), The sub-Alfvénic interaction of the Galilean satellites with the Jovian magnetosphere, *J. Geophys. Res.*, *103*, 19,843–19,866, doi:10.1029/97JE03370.

Raeder, J. (2003), Global magnetohydrodynamics—A tutorial, in *Space Plasma Simulation*, edited by J. Büchner, C. T. Dum, and M. Scholer, pp. 212–246, Springer, Berlin, New York.

Raeder, J. (2006), Flux transfer events: 1. Generation mechanism for strong southward IMF, *Ann. Geophys.*, *24*(1), 381–392, doi:10.5194/angeo-24-381-2006.

Raeder, J., and K. Germaschewski (2012), Algorithm to find quasi two-dimensional reconnection topology in three-dimensional simulations, in *Numerical Modeling of Space Plasma Flows: ASTRONUM-2011, Astron. Soc. Pac. Conf. Ser.*, vol. 459, edited by N. Pogorelov et al., p. 240, Astron. Soc. Pac., San Francisco, Calif.

Raeder, J., R. J. Walker, and M. Ashour-Abdalla (1995), The structure of the distinct geomagnetic tail during long periods of northward IMF, *Geophys. Res. Lett.*, *22*, 349–352, doi:10.1029/94GL03380.

Raeder, J., Y. L. Wang, and T. Fuller-Rowell (2001a), Geomagnetic storm simulation with a coupled magnetosphere-ionosphere-thermosphere model, in *Space Weather, Geophys. Monogr. Ser.*, vol. 125, edited by P. Song, G. Siscoe, and H. J. Singer, pp. 377–384, AGU, Washington, D. C.

Raeder, J., Y. L. Wang, T. J. Fuller-Rowell, and H. J. Singer (2001b), Global simulation of magnetospheric space weather effects of the Bastille Day storm, *Sol. Phys.*, *204*, 323–337, doi:10.1023/A:1014228230714.

Raeder, J., J. C. Dorelli, D. Larson, and B. Loring (2006), Physical, numerical, and computational challenges in modeling the geospace environment, in *Numerical Modeling of Space Plasma Flows, Astron. Soc. Pac. Conf. Ser.*, vol. 359, edited by N. Pogorelov and G. Zank, pp. 202–212, Astron. Soc. Pac., San Francisco, Calif.

Raeder, J., D. Larson, W. Li, E. L. Kepko, and T. Fuller-Rowell (2008), OpenGGCM simulations for the THEMIS mission, *Space Sci. Rev.*, *141*, 535–555, doi:10.1007/s11214-008-9421-5.

Raeder, J., P. Zhu, Y. Ge, and G. Siscoe (2010), Open geospace general circulation model simulation of a substorm: Axial tail instability and ballooning mode preceding substorm onset, *J. Geophys. Res.*, *115*, A00I16, doi:10.1029/2010JA015876.

Ridley, A., T. Gombosi, and D. Dezeeuw (2004), Ionospheric control of the magnetosphere: Conductance, *Ann. Geophys.*, *22*, 567–584, doi:10.5194/angeo-22-567-2004.

Ridley, A. J. (2007), Alfvén wings at Earth's magnetosphere under strong interplanetary magnetic fields, *Ann. Geophys.*, *25*, 533–542, doi:10.5194/angeo-25-533-2007.

Sarantos, M., and J. A. Slavin (2009), On the possible formation of Alfvén wings at Mercury during encounters with coronal mass ejections, *Geophys. Res. Lett.*, *36*, L04107, doi:10.1029/2008GL036747.

Saur, J. (2004), A model of Io's local electric field for a combined Alfvénic and unipolar inductor far-field coupling, *J. Geophys. Res.*, *109*, A01210, doi:10.1029/2002JA009354.

Saur, J., F. M. Neubauer, D. F. Strobel, and M. E. Summers (1999), Three-dimensional plasma simulation of Io's interaction with the Io plasma torus: Asymmetric plasma flow, *J. Geophys. Res.*, *1042*, 25,105–25,126, doi:10.1029/1999JA900304.

Saur, J., T. Grambusch, S. Duling, F. M. Neubauer, and S. Simon (2013), Magnetic energy fluxes in sub-Alfvénic planet star and moon planet interactions, *Astron. Astrophys.*, *552*, A119, doi:10.1051/0004-6361/201118179.

Schilling, N., F. M. Neubauer, and J. Saur (2008), Influence of the internally induced magnetic field on the plasma interaction of Europa, *J. Geophys. Res.*, *113*, A03203, doi:10.1029/2007JA012842.

Schunk, R. W., and A. F. Nagy (2000), *Ionospheres Physics, Plasma Physics and Chemistry*, Cambridge Univ. Press, Cambridge, U. K.

Shkolnik, E., G. A. H. Walker, and D. A. Bohlender (2003), Evidence for planet-induced chromospheric activity on HD 179949, *Astrophys. J.*, *597*, 1092–1096, doi:10.1086/378583.

Sibeck, D. G., G. L. Siscoe, J. A. Slavin, and R. P. Lepping (1986), Major flattening of the distant geomagnetic tail, *J. Geophys. Res.*, *91*, 4223–4237.

Usmanov, A. V., M. L. Goldstein, K. W. Ogilvie, W. M. Farrell, and G. R. Lawrence (2005), Low-density anomalies and sub-Alfvénic solar wind, *J. Geophys. Res.*, *110*, A01106, doi:10.1029/2004JA010699.

Zhang, B., W. Lotko, M. J. Wiltberger, O. J. Brambles, and P. A. Damiano (2011), A statistical study of magnetosphere-ionosphere coupling in the Lyon-Fedder-Mobarry global MHD model, *J. Atmos. Sol. Terr. Phys.*, *73*, 686–702, doi:10.1016/j.jastp.2010.09.027.